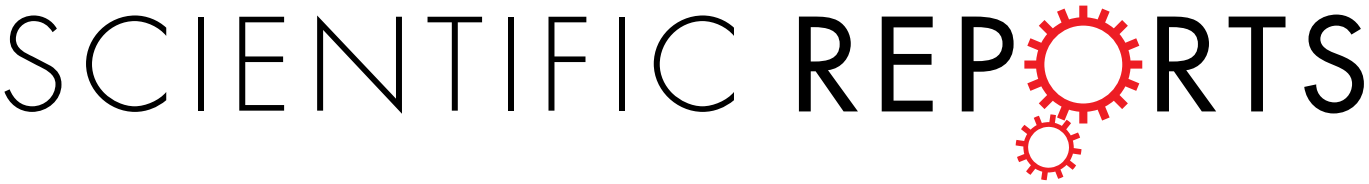

OPEN

Ca-α1T, a fly T-type Ca^{2+} channel, negatively modulates sleep

Kyunghwa Jeong[1], Soyoung Lee[2], Haengsoo Seo[2], Yangkyun Oh[1], Donghoon Jang[1], Joonho Choe[1], Daesoo Kim[1], Jung-Ha Lee[2] & Walton D. Jones[1]

Received: 11 August 2015
Accepted: 06 November 2015
Published: 09 December 2015

Mammalian T-type Ca^{2+} channels are encoded by three separate genes (Ca_v3.1, 3.2, 3.3). These channels are reported to be sleep stabilizers important in the generation of the delta rhythms of deep sleep, but controversy remains. The identification of precise physiological functions for the T-type channels has been hindered, at least in part, by the potential for compensation between the products of these three genes and a lack of specific pharmacological inhibitors. Invertebrates have only one T-type channel gene, but its functions are even less well-studied. We cloned Ca-α1T, the only Ca_v3 channel gene in *Drosophila melanogaster*, expressed it in *Xenopus* oocytes and HEK-293 cells, and confirmed it passes typical T-type currents. Voltage-clamp analysis revealed the biophysical properties of Ca-α1T show mixed similarity, sometimes falling closer to Ca_v3.1, sometimes to Ca_v3.2, and sometimes to Ca_v3.3. We found Ca-α1T is broadly expressed across the adult fly brain in a pattern vaguely reminiscent of mammalian T-type channels. In addition, flies lacking Ca-α1T show an abnormal increase in sleep duration most pronounced during subjective day under continuous dark conditions despite normal oscillations of the circadian clock. Thus, our study suggests invertebrate T-type Ca^{2+} channels promote wakefulness rather than stabilizing sleep.

T-type Ca^{2+} channels are a subfamily of voltage-dependent Ca^{2+} channels (VDCCs) that produce low-voltage-activated (LVA) Ca^{2+} currents implicated in NREM sleep in mammals[1]. Three different genes encode the pore-forming alpha subunits of mammalian T-type channels, Ca_v3.1, 3.2, and 3.3. Of these, Ca_v3.1 and 3.3 are highly expressed in the thalamus, where the oscillations required for NREM sleep are generated[2–4]. Mice lacking Ca_v3.1 show reduced delta-wave activity and reduced sleep stability, suggesting that mammalian T-type currents have a sleep-promoting or stabilizing function[1].

Unlike mammals, *Drosophila melanogaster* has only one T-type Ca^{2+} channel, Ca-α1T, which is also known as DmαG. A recent study found that motor neurons in flies lacking Ca-α1T show reduced LVA but also reduced high-voltage-activated (HVA) Ca^{2+} currents, suggesting that although Ca-α1T seems to be a genuine T-type channel, it may have interesting biophysical properties[5]. We therefore cloned a single isoform of Ca-α1T, expressed it in *Xenopus* oocytes or HEK-293 cells, and compared its biophysical properties with those of the rat T-type channel Ca_v3.1. We also generated several Ca-α1T mutant alleles and identified a defect in their sleep/wake cycles. Contrary to results in mammals, the fly T-type Ca^{2+} channel destabilizes sleep. We anticipate that our findings will help clarify species-dependent differences in the *in vivo* functions of T-type Ca^{2+} channels, particularly their role in sleep physiology.

Results

Ca-α1T produces LVA currents in *Xenopus* oocytes. The fly T-type Ca^{2+} channel Ca-α1T spans roughly 90 kilobases of genomic DNA and has five different annotated mRNA transcripts designated RB through RF. Because the smallest of these transcripts is still over 10 kilobases in length, we used a piece-meal approach to assemble a full-length cDNA. To do so, we isolated total RNA from fly heads and used reverse transcription to produce cDNAs. Using these cDNAs as a template, we amplified and then assembled partial clones to obtain full-length cDNAs for both the RB (NM_132068) and RC (NM_001103419) Ca-α1T transcripts. After sequence verification, we used these Ca-α1T cDNA clones to produce cRNAs for injection into *Xenopus* oocytes. We were able to confirm expression of the RC isoform, but not the RB isoform, by measuring robust inward currents using 10 mM Ba^{2+} as a charge carrier 4 days after cRNA injection. In all subsequent experiments performed with this RC isoform cDNA, we refer to it simply as Ca-α1T.

[1]KAIST, Department of Biological Sciences, Daejeon, 305-701, Republic of Korea. [2]Sogang University, Department of Life Sciences, Seoul, 121-742, Republic of Korea. Correspondence and requests for materials should be addressed to J.-H.L. (email: jhleem@sogang.ac.kr) or W.D.J. (email: waltonjones@kaist.edu)

We next compared the biophysical properties of Ca-α1T with those of a mammalian T-type Ca^{2+} channel homolog, rat $Ca_v3.1$[6], using the *Xenopus* oocyte expression system. Both Ca-α1T and $Ca_v3.1$ have low-voltage activation thresholds, but the threshold of Ca-α1T (-60 mV) is slighty lower than that of the rat channel by 3 ~ 4 mV. Both Ca-α1T and $Ca_v3.1$ produce current kinetics typical of T-type Ca^{2+} channels when subjected to a protocol of serial step pulses from a holding potential of -90 mV. Although the inactivation kinetics of Ca-α1T are slightly slower than those of $Ca_v3.1$, both the activation and inactivation kinetics of currents through Ca-α1T accelerate at higher step pulse values. This produces the criss-crossing pattern typical of T-type Ca^{2+} channels (Fig. 1a). Together, these biophysical properties—an activation threshold of -60 mV, a potential of maximal current at -20 mV, transient current kinetics, a criss-crossing pattern in currents evoked by a step pulse voltage protocol—all of these properties mark Ca-α1T as a typical T-type Ca^{2+} channel[6–9].

We next obtained activation curves for Ca-α1T and $Ca_v3.1$ by fitting chord conductances with the Boltzmann equation. The potential for half-maximal activation ($V_{50,act}$) of Ca-α1T and $Ca_v3.1$ are -43.32 ± 1.58 and -38.92 ± 1.15 mV, respectively. This indicates that Ca-α1T is activated at 4.4 mV lower test potentials than $Ca_v3.1$ ($p < 0.05$, Student's t-test) (Fig. 1b and Table 1). During steady-state inactivation, the potentials of 50% channel availability ($V_{50,\,inact}$) for Ca-α1T and $Ca_v3.1$ are estimated to be -58.04 ± 0.71 and -61.31 ± 0.70 mV ($p < 0.05$, Student's t-test). In other words, the $V_{50,inact}$ of Ca-α1T is 3.3 mV more positive than that of $Ca_v3.1$ (Fig. 1b and Table 1). An ion channel's so-called "window current" is the range of overlap in its activation and steady-state inactivation curves. This window for Ca-α1T is considerably larger than that of $Ca_v3.1$, implying that Ca-α1T is capable of persistently passing larger currents over the relevant voltage range than $Ca_v3.1$.

The voltage-dependent kinetics of the three mammalian T-type calcium channels are known to differ, with $Ca_v3.1$ and $Ca_v3.2$ showing faster activation/inactivation kinetics than $Ca_v3.3$[10]. To compare the time constants of activation and inactivation for Ca-α1T and $Ca_v3.1$, we fitted current traces with a double exponential function. At test potentials ranging from -50 mV to $+20$ mV, Ca-α1T has slower current kinetics than $Ca_v3.1$ ($p < 0.01$ for τ_{act} and $p < 0.001$ for τ_{inact}, Student's t-test, Fig. 1c). For example, the activation and inactivation time constants of Ca-α1T current at a -20 mV test potential are 2.2 ± 0.2 ms and 23.4 ± 1.4 ms respectively, whereas the activation and inactivation time constants of $Ca_v3.1$ current at the same test potential are 1.1 ± 0.2 ms and 9.7 ± 0.9 ms, respectively. This means the activation and inactivation kinetics of Ca-α1T are 2-fold slower than those of rat $Ca_v3.1$, but still in the "fast" range (Table 1).

Another defining property of the LVA T-type calcium channels is that they deactivate much more slowly than HVA calcium channels[6,9,11]. To characterize the deactivation kinetics of Ca-α1T, we performed a transient transfection of the Ca-α1T cDNA into HEK-293 cells followed by whole-cell patch clamp recordings of tail currents. As expected, the tail currents of Ca-α1T appear to undergo a slow voltage-dependent decay (Fig. 1d). The deactivation time constant obtained for Ca-α1T (0.93 ± 0.14 ms) by curve-fitting the tail currents is in the same range as that reported for all three mammalian Ca_v3 isoforms (Table 1).

Previous studies have shown that $Ca_v3.1$ passes larger amplitude currents when Ca^{2+} is used as a charge carrier rather than equimolar Ba^{2+}, but that the opposite is true for $Ca_v3.2$ and $Ca_v3.3$[12,13]. We, thus, measured the relative permeability of Ca-α1T and $Ca_v3.1$ to Ca^{2+} and Ba^{2+} ions (I_{Ca}/I_{Ba}). Consistent with previous reports, we measured a I_{Ca}/I_{Ba} ratio for $Ca_v3.1$ of 1.55 ± 0.03. This means the peak current amplitude of $Ca_v3.1$ is greater in 10 mM Ca^{2+} than 10 mM Ba^{2+} (Fig. 1e). The I_{Ca}/I_{Ba} ratio for Ca-α1T, however, is 0.68 ± 0.04. This means Ca-α1T passes a smaller current in 10 mM Ca^{2+} than in 10 mM Ba^{2+} (Fig. 1e). We also compared the relative permeability of Ca-α1T and $Ca_v3.1$ to these two divalent cations by comparing their maximal slope conductance ratios (G_{MaxCa}/G_{MaxBa}). The G_{MaxCa}/G_{MaxBa} ratios for Ca-α1T and $Ca_v3.1$ are 0.71 ± 0.10 (n = 6) and 1.43 ± 0.17 (n = 4), respectively (Fig. 1e). Thus, in terms of its relative permeability to Ca^{2+} and Ba^{2+}, Ca-α1T is more similar to $Ca_v3.2$ or $Ca_v3.3$ than $Ca_v3.1$ (Table 1).

Finally, T-type channel isoforms are also known to be differentially sensitive to blockage by Ni^{2+} ions, with $Ca_v3.2$ being the most sensitive of the three Ca_v3 isoforms[14]. Low micromolar levels of Ni^{2+} produce a concentration-dependent inhibition of Ca-α1T ($IC_{50} = 5.12\ \mu M$), while much higher levels of Ni^{2+} are necessary for blockage of $Ca_v3.1$ ($IC_{50} = 276.5\ \mu M$) (Fig. 1f). Thus, in terms of Ni^{2+} sensitivity, Ca-α1T more closely resembles $Ca_v3.2$ than $Ca_v3.1$ (Table 1).

Ca-α1T is broadly expressed in the adult brain. After several failed attempts to generate an antibody that works well for immunohistochemistry, we decided to tag the endogenous Ca-α1T with GFP and then visualize its expression pattern in the adult brain. First, we generated a founder line, (*Ca-α1T*$^{Founder,\ w+}$), using end-out homologous recombination to facilitate the versatile generation of a variety of different alleles[15] (Fig. 2a). In *Ca-α1T*$^{Founder,\ w+}$ flies, an *attP* landing site for ϕC31-mediated DNA integration and a floxed *white*$^+$ marker replace ~2 kb of genomic DNA surrounding the first coding exon of Ca-α1T. Next, we removed the *white*$^+$ marker from the *Ca-α1T*$^{Founder,\ w+}$ line by Cre-mediated recombination to generate *Ca-α1T*$^{Founder,\ w-}$. We then used the ϕC31 integrase to insert into the *attP* landing site of *Ca-α1T*$^{Founder,\ w-}$ an *attB* vector (*pGE-attB*^{GMR}) containing the deleted genomic region plus an additional GFP coding sequence and linker sequence in-frame after the start codon of Ca-α1T. This produced the *GFP::Ca-α1T* line, which expresses an N-terminally GFP-tagged Ca-α1T under the control of its own endogenous promoter.

Although *w*^{1118} control flies show no fluorescent background (Supplementary Fig. S1), these *GFP::Ca-α1T* flies show GFP fluorescence broadly across the brain (Fig. 2b). *GFP::Ca-α1T* is expressed in well-structured neuropils like the antennal lobes, the mushroom bodies, the central complex (Fig. 2c–h), the optic lobes, as well as in some of the less-structured neuropils. The central complex—comprising the fan-shaped body, ellipsoid body, noduli, and protocerebral bridge—shows the strongest expression with the ventral fan-shaped body and ventral noduli particularly prominent (Fig. 2e,g). In mushroom body neurons, there is far more *GFP::Ca-α1T* in the dendrite-rich calyx of the dorso-posterior brain (Fig. 2h) than the axon-rich lobes of the anterior brain (Fig. 2d). *GFP::Ca-α1T* is also limited to the posterior mushroom body peduncles, which are the fiber tracks that join the posterior calyces

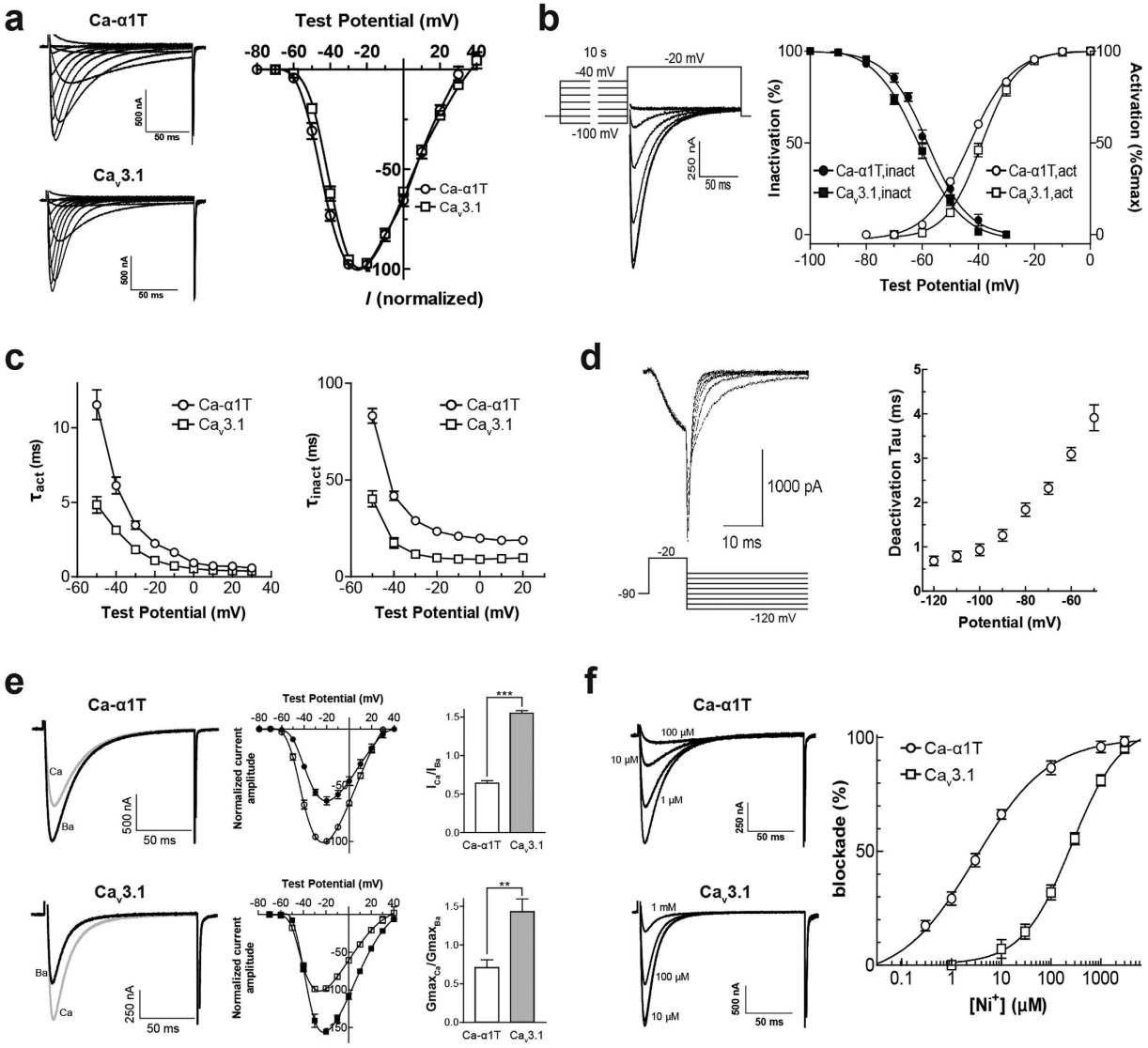

Figure 1. Comparing the biophysical properties of Ca-α1T and rat Ca$_v$3.1. (**a**) (Left) Representative current traces through Ca-α1T and Ca$_v$3.1 expressed in *Xenopus* oocytes. In 10 mM Ba^{2+}, currents were elicited by depolarizing 10 mV step pulses (−70 mV to +40 mV) from a holding potential of −90 mV. (Right) I–V relationships of Ca-α1T and Ca$_v$3.1. Peak currents for each oocyte were normalized to the maximum current. Percent amplitudes from oocytes expressing Ca-α1T (○) or Ca$_v$3.1 (□) plotted against test potentials and fitted with the Boltzmann equation. (**b**) (Left) Steady-state inactivation measured during voltage steps to −20 mV after 10 s prepulses to potentials between −100 mV and −40 mV. (Right) Voltage-dependent activation and steady-state inactivation curves of Ca-α1T (○, ●) and Ca$_v$3.1 (□, ■) fitted to the Boltzmann equation. (**c**) The activation (τ_{act}) and inactivation (τ_{inact}) time constants for Ca-α1T (○) and Ca$_v$3.1 (□) obtained by fitting the current traces to double exponentials. (**d**) Voltage-dependent deactivation of Ca-α1T in HEK-293 cells. Tail currents elicited by step pulses to −20 mV for 10 ms, followed by re-polarizing potentials (−120 mV to −50 mV). Deactivation time constants were obtained by fitting the traces to a single exponential and plotted against re-polarizing potentials. (**e**) I_{Ca}/I_{Ba} ratios of Ca-α1T and Ca$_v$3.1. (Left) Representative current traces through Ca-α1T and Ca$_v$3.1 measured in 10 mM Ba^{2+} or 10 mM Ca^{2+} elicited by 10 mV step pulses from a holding potential of −90 mV. Ba^{2+} currents are black; Ca^{2+} currents are grey. (Middle) I–V relationships of Ca-α1T (○, ●) and Ca$_v$3.1 (□, ■) in 10 mM Ba^{2+} (open) or 10 mM Ca^{2+} (filled). (Right) Peak current ratios (I_{Ca}/I_{Ba}) and relative slope conductance (G_{MaxCa}/G_{MaxBa}) for Ca-α1T and Ca$_v$3.1. Student's t-test, $^{**}p < 0.01$, $^{***}p < 0.001$. (**f**) Nickel inhibition sensitivity of Ca-α1T and Ca$_v$3.1. (Left) Representative current traces of Ca-α1T and Ca$_v$3.1 at various Ni^{2+} concentrations. (Right) Dose-response curves indicating Ni^{2+}-dependent inhibition of Ca-α1T (○) and Ca$_v$3.1 (□). Data are presented as means ± s.e.m.

with the anterior mushroom body lobes (Fig. 2f). These results suggest strict regulation of the subcellular localization of Ca-α1T channels in the brain.

We next visualized the projections of Ca-α1T-expressing neurons using another knock-in allele, *Ca-α1T^{Gal4}*. In *Ca-α1T^{Gal4}*, the first coding exon and flanking introns of Ca-α1T are replaced by the Gal4 coding sequence. This

	Ca-α1T	*Rat $Ca_v3.1$*	*$Ca_v3.1$*	*$Ca_v3.2$*	*$Ca_v3.3$*
Activation					
V_{50} (mV)	−43.3 ± 1.6 (11)	−38.9 ± 1.2 (14)	**−40.0 ± 0.8**[49]	−36.2 ± 0.6[49]	−29.1 ± 1.3[49]
k (mV)	7.7 ± 1.3 (11)	6.4 ± 0.9 (14)	NA	NA	NA
Inactivation					
V_{50} (mV)	−58.0 ± 0.7 (5)	−61.3 ± 0.7 (15)	−64.9 ± 0.7[49]	−62.0 ± 0.9[49]	**−55.6 ± 0.9**[49]
Current kinetics (−20 mV)					
τ_{act} (ms)	2.2 ± 0.2 (10)	1.1 ± 0.2 (5)	**1.4 ± 0.1**[50]	3.2 ± 0.1[51]	22.8 ± 1.5[50]
τ_{inact} (ms)	23.4 ± 1.4 (6)	9.7 ± 0.9 (5)	7.2 ± 0.4[50]	**11.6 ± 0.2**[51]	97.0 ± 3.8[50]
Deactivation kinetics (−100 mV)					
τ_{deact} (ms)	0.9 ± 0.1 (6)[a]	NA	2.6 ± 0.2[52a,b]	3.6 ± 0.4[52a,b]	**1.12 ± 0.1**[52a,b]
Conductance					
I_{Ca}/I_{Ba}	0.7 (6)	1.6 (3)	1.5[13]	0.8[13]	**0.7**[13]
Pharmacology					
Ni^{2+} (IC_{50} μM)	5.1 (6–12)	276.5 (5–6)	167 ± 15[14c]	**5.7 ± 0.3**[14c]	87 ± 7[14c]

Table 1. Comparison of the biophysical properties of Ca-α1T and mammalian T-type calcium channels. V_{50}, potential of half maximal activation or inactivation. *k*, slope factor from the Boltzmann equation. Number of oocytes is in parentheses. The measurements reported in the first two columns labeled Ca-α1T and Rat $Ca_v3.1$ were measured in this study, while the final three columns are from published reports. Bold-faced entries in the final three columns denote the mammalian T-type channel properties that most closely match the measured properties of Ca-α1T. NA, not available. [a]Recorded in HEK-293 cells. [b]2 mM Ca^{2+} instead of 10 mM Ba^{2+} as charge carrier. [c]−30 mV as repolarizing potential.

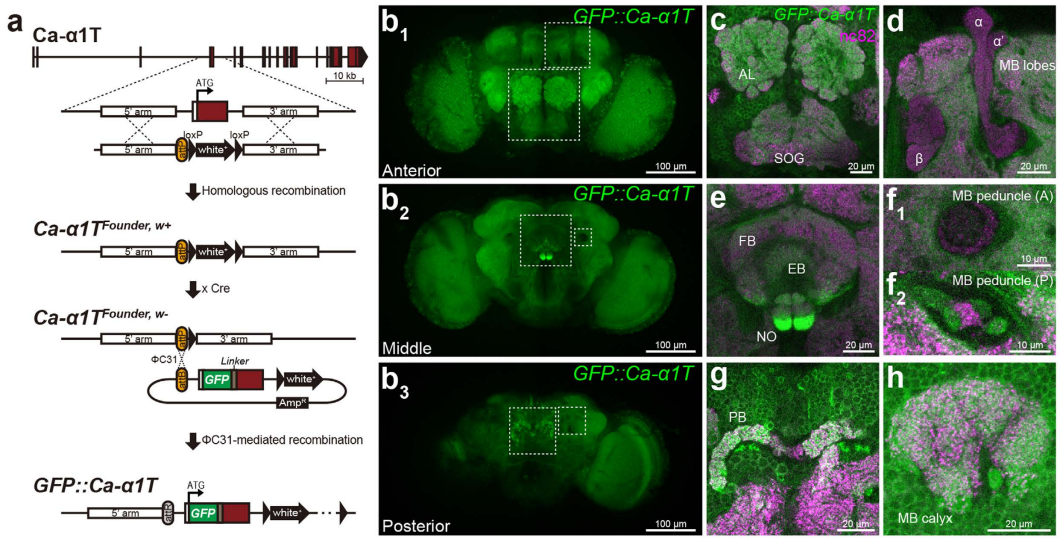

Figure 2. GFP::Ca-α1T expression in the adult brain. (**a**) Gene targeting and *GFP::Ca-α1T* generation strategy. Ca-α1T coding exons are red. (**b**) Adult brain expression of *GFP::Ca-α1T* (green) divided into maximal intensity projections of confocal stacks from the anterior (**b1**), middle (**b2**), and posterior (**b3**) brain. (**c–h**) GFP::Ca-α1T expression in specific neuropils whose location corresponds to the boxed areas in (**b**). (**c**) Expression in the antennal lobes (AL) and subesophageal ganglia (SOG). (**d**) Expression in the mushroom body (MB) lobes (α, β, and α'). (**e**) Expression in the fan-shaped body (FB), ellipsoid body (EB), and noduli (NO) of the central complex. (**f**) Expression in the (**f1**) anterior and (**f2**) posterior mushroom body (MB) peduncles. (**g**) Expression in the protocerebral bridge (PB) of the central complex. (**h**) Expression in the mushroom body (MB) calyx. Neuropils are counter-stained with the nc82 antibody (α-Bruchpilot, magenta).

puts GAL4 expression under the control of the endogenous Ca-α1T promoter (Fig. 3a). Consistent with our results using *GFP::Ca-α1T*, *Ca-α1T^{Gal4}* drives the expression of a membrane-tethered mCherry (*UAS-mCD8-ChRFP*) broadly across the brain (Supplementary Fig. S2). The *Ca-α1T^{Gal4} > mCherry* and *GFP::Ca-α1T* signals are strongly co-localized, including in the central complex and mushroom bodies (Supplementary Fig. S2). This suggests both reagents reflect proper expression from the same endogenous Ca-α1T promoter.

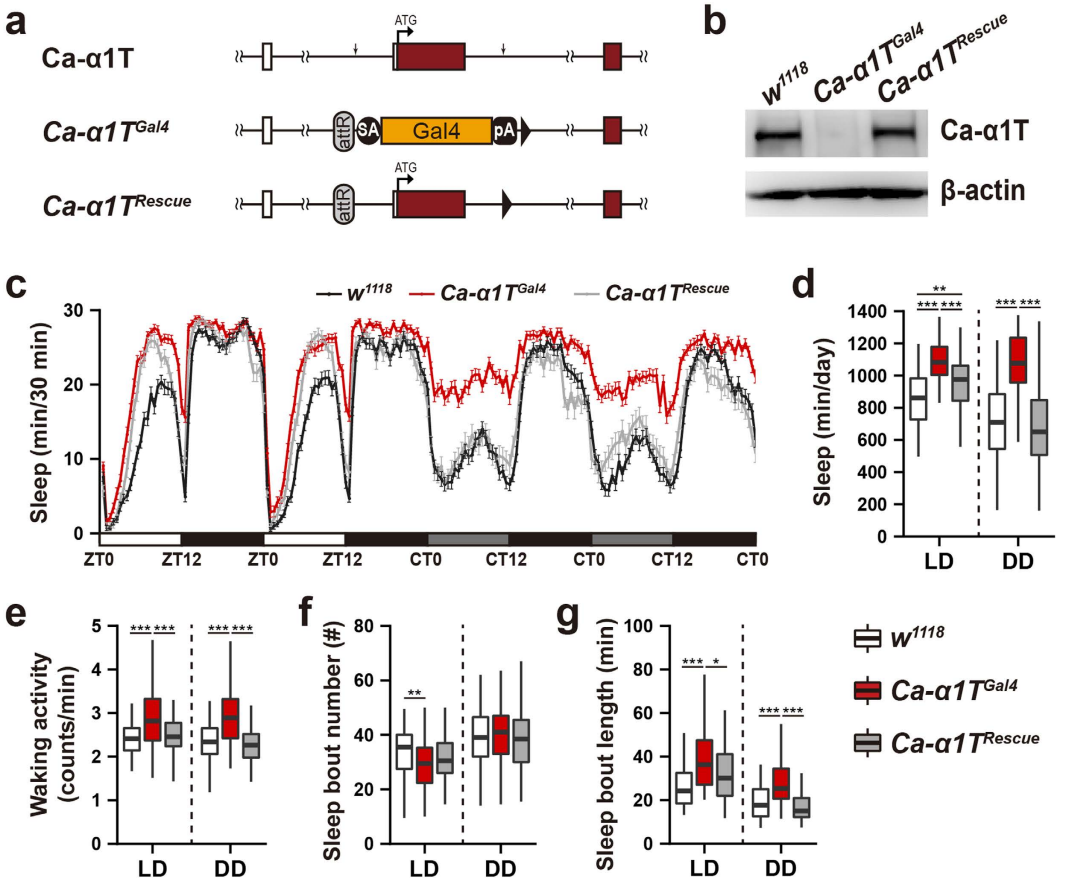

Figure 3. Sleep is increased in *Ca-α1T* mutants. (**a**) *Ca-α1T*, *Ca-α1T*^{Gal4}, and *Ca-α1T*^{Rescue} schematics. Ca-α1T coding exons are red. Downward arrows denote the extent of the deleted region. SA, splice acceptor. pA, polyA sequence. (**b**) Western blot analysis of Ca-α1T protein levels of fly head lysates. Ca-α1T is undetectable in *Ca-α1T*^{Gal4} lysates while *Ca-α1T*^{Rescue} lysates show levels similar to the *w*^{1118} control. β-actin was used as a loading control. (**c**) Sleep profiles of *w*^{1118} (black, n = 89), *Ca-α1T*^{Gal4} (red, n = 92) and *Ca-α1T*^{Rescue} (grey, n = 61) over two days of 12 h:12 h light-dark (LD) and two days of continuous dark (DD) conditions. Sleep is plotted in 30 minute intervals. Data are presented as means ± s.e.m. White, black, and grey bars denote light phase, dark phase, and subjective light phase, respectively. ZT, zeitgeber time. CT, circadian time. (**d**) Total daily sleep under LD and DD conditions. (**e**) Waking activity under LD and DD conditions measured as total activity counts divided by waking minutes. (**f**) The number of sleep bouts under LD and DD conditions. (**g**) Average sleep bout length under LD and DD conditions. Boxplot whiskers extend to the highest and lowest values that fall within 1.5× IQR of the upper and lower quartiles. All indications of statistical significance were determined using Welch's ANOVA followed by the Games-Howell post hoc test. $*p < 0.05$, $**p < 0.01$, $***p < 0.001$.

Ca-α1T mutants show increased sleep. Since the Gal4 coding sequence inserted into *Ca-α1T*^{Founder} to produce the *Ca-α1T*^{Gal4} allele included a termination sequence (Fig. 3a), *Ca-α1T*^{Gal4} is likely a null allele. As expected, we were unable to detect Ca-α1T expression in the fly head lysates from *Ca-α1T*^{Gal4} in western blot analyses using polyclonal Ca-α1T-specific antisera (Fig. 3b). We did, however, detect strong Ca-α1T expression in lysates from *w*^{1118} controls and from a *Ca-α1T*^{Rescue} allele in which the fragment deleted in both the *Ca-α1T*^{Founder} and *Ca-α1T*^{Gal4} alleles was re-inserted (Fig. 3a,b). *Ca-α1T*^{Gal4} homozygotes are viable and fertile with normal appearance and no obvious movement defects. Two of the mammalian T-type channel subtypes, $Ca_v3.1$ and $Ca_v3.3$, have been implicated in the generation of the neural oscillations characteristic of NREM sleep[1,16]. Flies have a well-established sleep-like state that shares some features with mammalian sleep, but it remains unclear whether flies have a stage akin to mammalian NREM sleep. Still, we hypothesized that Ca-α1T-null flies may exhibit sleep defects.

Ca-α1T^{Gal4} flies show increased total sleep under both 12 h:12 h light-dark (LD) and constant dark (DD) conditions, but this phenotype is particularly prominent during the subjective day under continuous dark (DD) conditions (Fig. 3c,d). The total sleep of *Ca-α1T*^{Rescue} flies shows a partial rescue in light-dark (LD) conditions and a full rescue to *w*^{1118} levels under continuous darkness (DD) (Fig. 3c,d). Although levels of Ca-α1T protein are grossly normal in *Ca-α1T*^{Rescue} flies (Fig. 3b), it is possible that the addition of the attR site and the loxP sites in the *Ca-α1T*^{Rescue} allele (Fig. 3a) subtly reduce expression of Ca-α1T in some small but important neuronal subpopulation preventing a full rescue. By measuring waking locomotor activity, we were able to confirm that the increased sleep of *Ca-α1T*^{Gal4} flies is not an artifact of a generalized reduction in movement. In fact, *Ca-α1T*^{Gal4} show slightly higher levels of waking activity than their respective controls (Fig. 3e).

Normal fly sleep consists of a number of sleep bouts. We, therefore, asked whether the increased sleep of *Ca-α1T*^{Gal4} flies is a result of an increased number of sleep bouts, prolonged bout duration, or both. *Ca-α1T*^{Gal4} flies do show reduced sleep bout number under LD conditions, but this phenotype is not rescued in *Ca-α1T*^{Rescue} flies (Fig. 3f). Sleep bout length, on the other hand, is increased under both LD and DD conditions and rescued in *Ca-α1T*^{Rescue} flies (Fig. 3g).

To confirm that this elevated sleep phenotype is specific to Ca-α1T loss-of-function, we generated three independent deletion mutants via imprecise P-element excision. As expected, all three deletion mutants as well as a trans-heterozygous mutants (Δ3/Δ115) show increased sleep, especially in constant darkness (Supplementary Fig. S3). In addition, knockdown of Ca-α1T in its own neurons (*Ca-α1T*^{Gal4} > *UAS-Ca-α1T-IR*) increases sleep after the third day of continuous darkness (Supplementary Fig. S4). Together, these results implicate Ca-α1T as a novel inhibitor of fly sleep.

Circadian rhythms and sleep homeostasis of Ca-α1T mutants. As in other animals, sleep in *Drosophila* is regulated by the circadian clock, meaning clock mutants generally show altered sleep phenotypes[17,18]. We therefore asked whether the increased sleep observed in Ca-α1T-null flies can be attributed to a disruption of the circadian clock. After monitoring locomotor activity over seven days of continuous darkness, we found that most *Ca-α1T*^{Gal4} flies have a slightly elongated circadian period length (24.3 ± 0.6 vs. 23.9 ± 0.2), a significantly reduced power of rhythmicity (22.3 ± 2.9 vs. 53.4 ± 5.1), and a reduced overall percentage of rhythmic flies (70.3% vs. 92.6%) when compared to *w*^{1118} controls (Fig. 4a). This circadian phenotype of *Ca-α1T*^{Gal4} flies is unlikely due to problems in the core circadian clock, however, as transcriptional oscillation of *period* is normal (Fig. 4b). This means Ca-α1T must act downstream of the core circadian clock to affect rhythmic behaviors, perhaps affecting the firing of important clock-related neurons.

In addition to being controlled by the circadian clock, sleep is also associated with a homeostatic drive proportional to the time an animal spends awake. Thus, we next examined this homeostatic sleep drive in *Ca-α1T*^{Gal4} flies by depriving them of sleep for 24 hours and measuring the resulting sleep rebound. *Ca-α1T*^{Gal4} flies do recover slightly more of their lost sleep than *w*^{1118} controls, but the difference is not statistically significant (Fig. 4c).

Pan-neuronal knock-down of Ca-α1T increases sleep. We next asked whether the increased sleep phenotype of *Ca-α1T*^{Gal4} flies can be attributed to the function of Ca-α1T in the brain. Pan-neuronal knock-down of Ca-α1T (*elav-Gal4* > *UAS-Ca-α1T-IR*) increases sleep beyond that of heterozygous controls under both LD and DD conditions (Fig. 5). Using the drug-inducible GeneSwitch-Gal4 technique[19], we asked whether Ca-α1T's influence on sleep occurs during development or whether it is limited to its expression in the adult brain. Ca-α1T knock-down using *elav-GeneSwitch(GS)-Gal4* increases sleep in continuous darkness when compared to non-induced controls (Supplementary Fig. S5). This suggests the sleep phenotype of Ca-α1T-null mutants are unlikely due to developmental defects.

Finally, we sought to narrow down the sleep-regulating role of Ca-α1T to a specific brain region or circuit. We used a range of neuronal Gal4 drivers that cover known sleep centers to knockdown Ca-α1T, but none of them were capable of significantly altering sleep (Fig. 6).

Discussion

In this study, we cloned the only voltage-gated T-type Ca^{2+} channel from *Drosophila*, Ca-α1T. Ca-α1T is the largest T-type channel cloned to date, measuring 3205 amino acids[20]. Electrophysiological characterization of Ca-α1T in *Xenopus* oocytes showed that Ca-α1T has the hallmark properties of a T-type channel: low-threshold activation at around −60 mV, a maximal current output at −20 mV, transient current kinetics elicited by a step-pulse protocol producing a "criss-crossing" pattern, and slow deactivation of tail currents (Fig. 1). These biophysical properties are also consistent with previous studies that implicated Ca-α1T in low-voltage-activated (LVA) currents in both the central and peripheral nervous systems of the fly[5,21].

Mammalian genomes contain three T-type Ca^{2+} channel genes (i.e., $Ca_v3.1$–3.3), while the fly genome contains only one. We therefore measured Ca-α1T for some of the characteristics that distinguish the three mammalian channels. In terms of current kinetics, Ca-α1T is more similar to mammalian $Ca_v3.1$ and $Ca_v3.2$ than $Ca_v3.3$, which exhibits considerably slower kinetics. In terms of both its relative permeability to Ba^{2+} over Ca^{2+} and its sensitivity to nickel inhibition, Ca-α1T is most similar to $Ca_v3.2$[22,23].

The three mammalian T-type Ca^{2+} channels, each with their own distinct biophysical properties, are expressed in largely complementary patterns of neurons throughout the brain, conferring considerable functional diversity. Areas of particularly strong expression include those important for the gating and processing of sensory inputs, motor control, learning and memory, as well as reward circuits[4]. Using a GFP-tagged knock-in allele, we report in this study that Ca-α1T is expressed broadly across the adult fly brain in structures reminiscent of the mammalian T-type Ca^{2+} channels. These include sensory neuropils (i.e., the optic and antennal lobes, the antennal mechanosensory and motor centers, the anterior ventrolateral protocerebrum, and the subesophageal zone), motor-associated neuropils (i.e., the central complex), and those associated with learning, memory, and reward (i.e., the mushroom bodies). It is still unclear, however, whether the different isoforms predicted to originate from the *Ca-α1T* locus will have different biophysical properties or different distributions around the brain.

Considering their broad expression, T-type knockout mice appear healthy and subtle mutant phenotypes emerge only upon close inspection. Sleep, in particular, has become a focal point in the search for a physiological function for the T-type channels. Mammalian T-type Ca^{2+} channels may act as sleep stabilizers and may help generate the burst firing necessary for the sleep oscillations of deep NREM sleep. Unfortunately, the three separate mammalian T-type genes all undergo alternative splicing to produce various channel isoforms that each have specific biophysical properties, neuroanatomical and subcellular localizations, and varying abilities to interact with other ion channels. All these variables and more combine to make it difficult if not impossible to define a

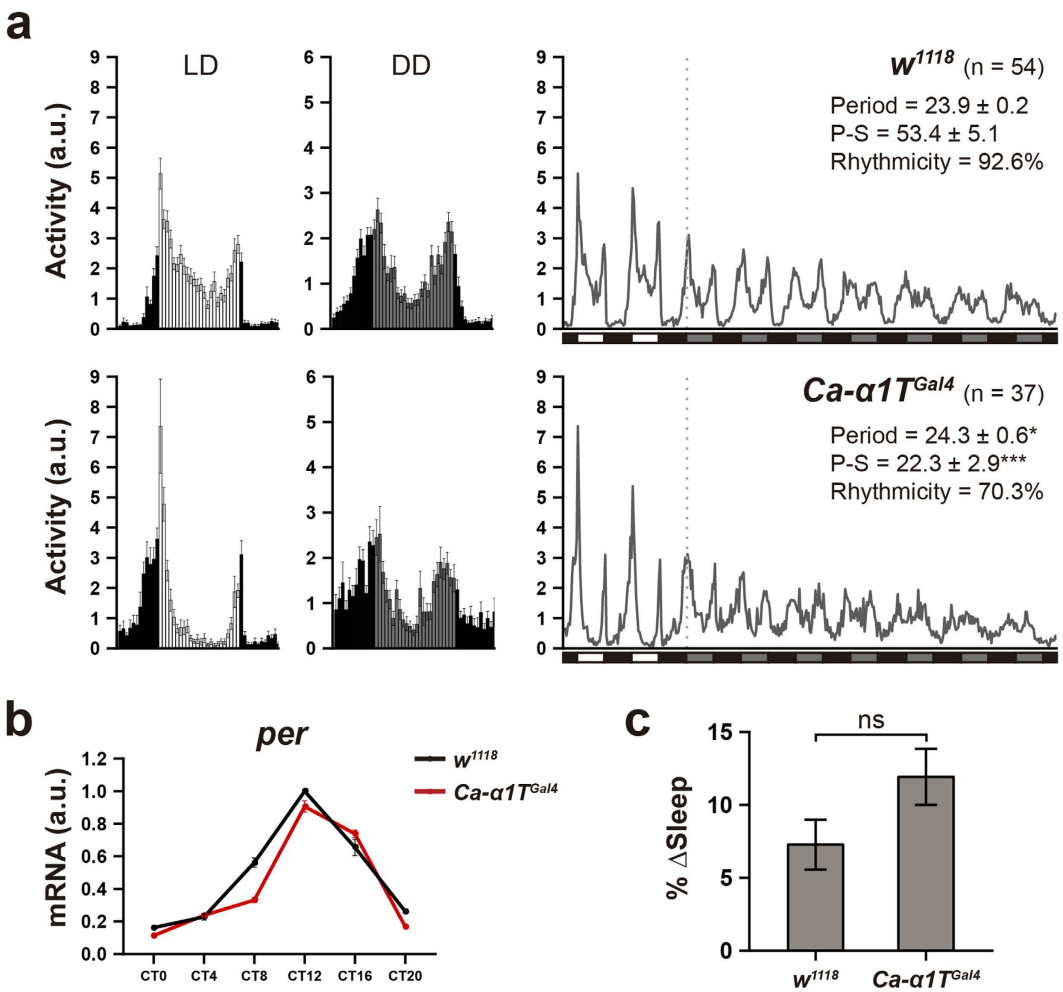

Figure 4. ***Ca-α1T*^{Gal4} flies show rhythmic locomotion and homeostatic regulation of sleep.** (**a**) Average activity profiles from day 2 of the 12 h:12 h light-dark cycles (LD, left), day 2 of continuous darkness (DD, middle), and from throughout the experiment (2 LD + 7 DD, right). In the left and middle panels, data are presented as means ± s.e.m. In the right panel, white, black, and grey bars indicate light phase, dark phase, and subjective light phase, respectively. The dotted line indicates the beginning of constant darkness. The number of flies measured, their rhythmic period, their power of rhythmicity (P-S), and the percentage of rhythmic flies (Rhythmicity) are indicated. a.u., arbitrary unit. The Mann-Whitney U test was used to determine the significance of the period changes ($^{*}p < 0.05$), while Welch's t-test was used for rhythmic power ($^{***}p < 0.001$). (**b**) Transcriptional oscillation of the *period* gene in *Ca-α1T*^{Gal4} under DD conditions. Black and red lines denote w^{1118} and *Ca-α1T*^{Gal4}, respectively. *rp49* was used for normalization. a.u., arbitrary unit. (**c**) Percentage of lost sleep recovered (% Δ Sleep) over a 12 hr period after 24 hours of mechanically-induced sleep deprivation. w^{1118} (n = 35) and *Ca-α1T*^{Gal4} (n = 33). Statistical significance was determined using the Student's t-test. ns, not significant. Data are presented as means ± s.e.m.

precise physiological role in sleep for T-type channels as a group. Although $Ca_v3.1$ knockout mice lack the delta oscillations characteristic of deep sleep and show reduced total sleep[1], when the knockout is limited to the rostral midline thalamus, sleep is still reduced, but delta waves are mildly increased[24]. Another more recent study showed that treatment with the T-type-specific channel blocker TTA-A2 enhances sleep and delta rhythms in wild type mice but not $Ca_v3.1/Ca_v3.3$ double knockout mice[25]. In other words, manipulation of T-type channels can both enhance and reduce total sleep and deep delta-wave sleep depending on the experimental context.

Although perhaps an underestimate of the actual complexity of the situation, the subtlety of the phenotypes of the homozygous viable Ca_v3 mutant mice are often ascribed to functional compensation among the various $Ca_v3.1–3$ isoforms[26]. We, therefore, expected that a behavioral investigation of the one and only fly T-type channel, Ca-α1T, would uncover less subtle sleep phenotypes. We were thus surprised to find, that despite its broad and relatively strong expression across adult fly brains, Ca-α1T-null mutants, like the $Ca_v3.1$-null mice, are homozygous viable and lack any overt phenotypes. Upon closer examination, however, we observed that Ca-α1T-null mutants sleep more than controls, especially in constant darkness.

The reason for this relative specificity in the sleep phenotype caused by Ca-α1T loss-of-function to constant darkness is still unclear. Flies exhibit a burst of activity upon exposure to the early morning light but then sleep

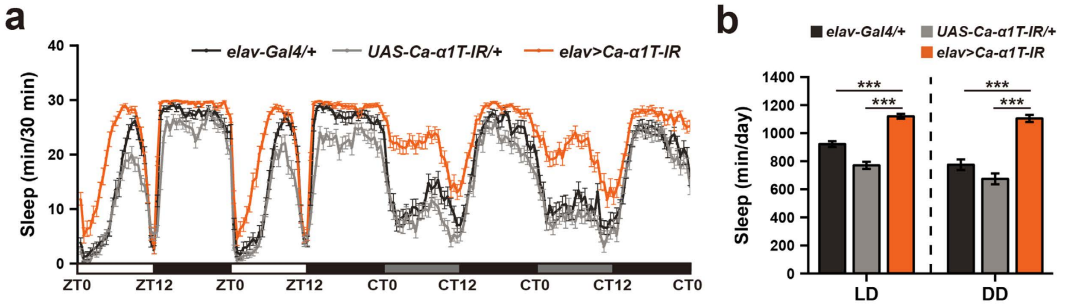

Figure 5. Pan-neuronal Ca-α1T knockdown increases sleep. (**a**) Sleep profiles of over two days of 12 h:12 h light-dark cycles (LD) and two days of continuous darkness (DD). Pan-neuronal knockdown of Ca-α1T (*elav > Ca-α1T-IR*, orange, n = 44) increases sleep beyond that of the heterozygous Gal4 control (*elav-Gal4/+*, black, n = 38) and the heterozygous UAS control (*UAS-Ca-α1T-IR/+*, grey, n = 42). Sleep is plotted in 30 minute intervals. White, black, and grey bars denote light phase, dark phase, and subjective light phase, respectively. ZT, zeitgeber time. CT, circadian time. (**b**) Quantification of average total sleep over two days of light-dark cycles (LD) and two days of continuous darkness (DD). Data are presented as means ± s.e.m. and analyzed via one-way ANOVA followed by the Tukey-HSD post hoc test. $^{***}p < 0.001$.

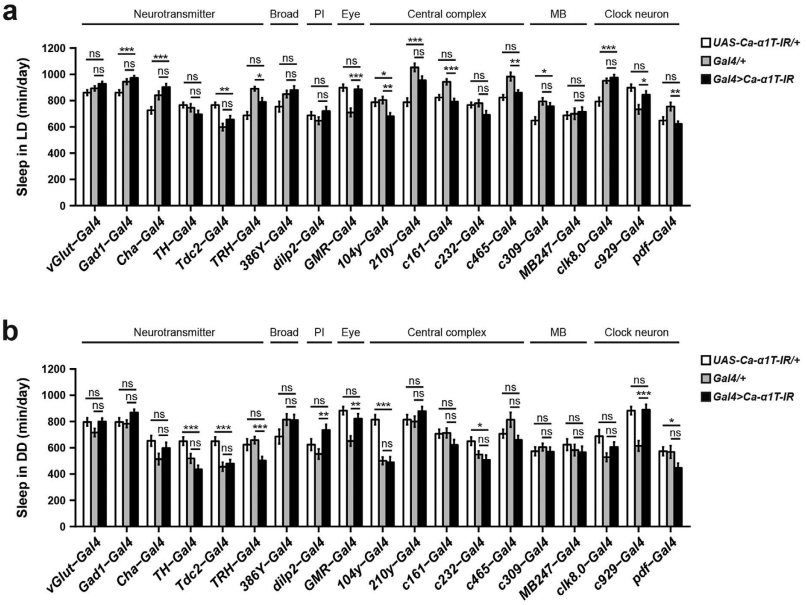

Figure 6. Knockdown of Ca-α1T in various neuronal subsets. (**a**) Average total sleep over two days of 12 h:12 h light-dark cycles (LD). (**b**) Average total sleep over two days of continuous darkness (DD). White, grey, and black bars denote *UAS-Ca-α1T-IR/+*, *Gal4/+* and *Gal4 > Ca-α1T-IR*, respectively (n = 21–83). PI, pars intercerebralis, MB, mushroom body. Data are presented as means ± s.e.m. Statistical significance was determined using Welch's ANOVA followed by the Games-Howell post hoc test. ns, not significant. $^{*}p < 0.05$, $^{**}p < 0.01$, $^{***}p < 0.001$.

through most of the rest of the day. Since control flies show less sleep during subjective daytime under continuous darkness than under the light phase of light-dark conditions (Fig. 3c), it is clear that light exposure can also have sleep-promoting effects. Through a series of imaging experiments, Shang *et al.* reported that although dopamine (DA) is potently wake-promoting, light exposure can suppress this action of DA at least partly by causing the up-regulation of the inhibitory DA receptor D2R in PDF neurons, which are themselves wake-promoting[27]. This modulation of the wake-promoting PDF neurons by light may help explain why the Ca-α1T loss-of-function phenotype is biased toward continuous dark conditions if Ca-α1T functions downstream of the PDF neurons. It would mean the responsible Ca-α1T-positive neurons are also modulated by light.

We were able to replicate the increased sleep phenotype of Ca-α1T-null mutants via pan-neuronal knock-down of Ca-α1T, but we were unable to further narrow the cause of this phenotype to a more specific neuronal subpopulation. This was in spite of numerous attempts with neuronal Gal4 driver lines ranging from broadly expressed enhancer traps and neurotransmitter Gal4 drivers to much more narrowly expressed neuropeptide drivers. This difficulty suggests Ca-α1T may function in novel sleep circuits.

In addition to their sleep phenotype, Ca-α1T-null mutants also have a circadian phenotype: an elongated circadian period and a reduction in rhythmic power. It is difficult to say, however, whether these altered circadian parameters are independent of or secondary to the sleep phenotype. Rhythmic power is proportional to the magnitude of the changes in activity level and the regularity with which they occur. Since the increased sleep observed in the Ca-α1T-null mutants does reduce the change in overall activity level between subjective day and subjective night, the increased sleep must also cause a reduction in rhythmic power.

The length of time animals spend sleeping is controlled by both the circadian clock and by a homeostatic drive to sleep that is proportional to time spent awake. Thus, most "sleep mutants" described so far have had defects in one or the other—they are either circadian sleep mutants or homeostatic sleep mutants. After 24 hours of mechanically-induced sleep deprivation, we observed that Ca-α1T-null mutants re-gain slightly more of their lost sleep than control flies (Fig. 4c), although the increase was not statistically significant. This suggests that, in addition to their circadian phenotype, Ca-α1T-null mutants may also have a slightly stronger homeostatic drive to sleep than controls. Although neither the circadian phenotype nor the homeostatic phenotype are particularly strong, together they produce a robust increase in sleep.

The "three channel" compensation hypothesis in mice may yet turn out to be correct, but our results in flies suggest that other factors—isoform-specific differences, differences related to protein–protein interactions, or even something completely unforeseen—may allow mice and flies lacking these broadly expressed and highly conserved ion channels to still function remarkably well. It will be interesting to see whether future studies focused on the technically demanding study of isoform-specific expression patterns and isoform-specific rescues in both mice and flies will clarify how T-type channels can at various times and in various contexts both enhance and reduce sleep.

Methods

Fly stocks. Flies were kept on a standard corn meal, corn syrup, yeast, and agar medium at room temperature. *UAS-mCD8-ChRFP* (#27392), *vGlut-Gal4* (#26160), and *Gad1-Gal4* (#47140) were newly obtained from the Bloomington Drosophila Stock Center (Indiana, USA) for these experiments. The UAS-Ca-alpha1T-IR line (#48008) was obtained from the Vienna Drosophila RNAi Center. EP line G1047 was obtained from Genexel. *c465-Gal4* and *210y-Gal4* were gifts from J. Douglas Armstrong[28]. The following stocks were all described previously: *elav-Gal4*[29], *elav-GS-Gal4*[19], *Cha-Gal4*[30], *104y-Gal4*[31], *c309-Gal4*[32], *MB247-Gal4*[33], *pdf-Gal4*[34], *TH-Gal4*[35], *GMR-Gal4*[36], *clk8.0-Gal4*[37], *dilp2-Gal4*[38], *Tdc2-Gal4* and *TRH-Gal4*[39], *c161-Gal4* and *c232-Gal4*[40], and *c929-Gal4* and *386Y-Gal4*[41].

Cloning Ca-α1T. We generated a full-length Ca-α1T (CG15899) cDNA by piecemeal PCR amplification. Total RNA extracted from adult heads using Trizol reagents (Invitrogen) was reverse transcribed using RevertAid First Strand cDNA Synthesis Kit (Fermentas). Six adjacent DNA fragments that cover the entire Ca-α1T cDNA were obtained by PCR amplification. Primer sets were designed based on the FlyBase (FB2011_07) annotation for Ca-α1T. Hind III and Xba I sites were inserted at the 5′ end of fragment 1 and 3′ end of fragment 6, respectively. Primer sets: fragment 1 (5′-CGAGATAAGCTTAAAATGCTGCCACAGCCA-3′, 5′-GCATCAGACTACATCGCTGTC-3′), fragment 2 (5′-CTGGACACGCTGCCCATGCTG-3′, 5′-TTCCAGCTCCTCCACTTGCAC-3′), fragment 3 (5′-CAACGGTGGCTCCAACAGTCG-3′, 5′-CCACTGGCGGAAGCTCATGCC-3′), fragment 4 (5′-GCCACGCCTCTCCAAGATCCG-3′, 5′-GACGATAAGAGCGTTTGCACG-3′), fragment 5 (5′-TCTGAAACTAGTCGTGCAAAC-3′, 5′-TGGAAGTACTGGACGGTCTGC-3′), and fragment 6 (5′-AATCCCAGCCTGACCAGCTCG-3′, 5′-TCTAGATTAGTCCATGGAGGATTGGGGTGA-3′). Amplified PCR fragments were sequenced and assembled into pBlueScript II KS (+) using sequential restriction enzyme digests. Clones 2 and 3 contained isoform-specific exons. Of the combinations that were amplified by PCR, we chose to proceed to assembling the RB and RC isoforms. We observed frequent, but inconsistent mutations and instances of A to G RNA editing in fragments 3 and 5. To achieve a final Ca-α1T cDNA matching the FlyBase annotation, we reverted one edited site in fragment 3 (5′-AGTTCAGAGC-3′) by site-directed mutagenesis. Since fragment 5 had so many inconsistencies and contained no introns, we used genomic DNA as a template for fragment 5 instead of cDNA. The final assembled full-length cDNAs were cut with HindIII/XbaI and subcloned into pcDNA3-HE3 downstream of the 5′-UTR from the *Xenopus laevis* β-globin gene to improve expression in *Xenopus* oocytes.

Chemicals and preparation of solutions. Most of the chemicals for electrophysiological recordings were purchased from Sigma-Aldrich (St. Louis, MO, USA). A 100 mM nickel-chloride stock solution was made in deionized water. A series of nickel solutions (in μM: 0.3, 1, 3, 10, 30, 100, 300, 1000, and 3000) were prepared by diluting the stock solution with 10 mM Ba^{2+} recording solution (in mM: 10 BaOH2, 90 NaOH, 1 KOH, 5 HEPES, pH 7.4 adjusted with methanesulfonic acid) before every nickel inhibition experiment.

Functional expression of T-type channels in *Xenopus* oocytes. Linearized cDNAs encoding rat $Ca_v3.1$ or Ca-α1T were used as templates for the synthesis of capped cRNAs using T7 RNA polymerase (Ambion, Austin, TX, USA). cRNA concentrations were estimated based on spectrophotometric optical density measurements at 260 nm. Oocyte preparation from female *Xenopus laevis* and injection of cRNAs was performed as previously reported[22]. GenBank accession numbers: rat $Ca_v3.1$ (α_1G), AF027984[6]; Ca-α1T C isoform, NP001096889.

Electrophysiology. Ba^{2+} (or Ca^{2+}) currents through T-type channels expressed in oocytes were measured at room temperature 4–5 days after cRNA injection using a two-electrode voltage-clamp amplifier (OC-725C, Warner Instruments, Hamden, CT, USA). Microelectrodes were pulled from capillaries (G100TF-4, Warner Instruments, Hamden, CT, USA) using a pipette puller and filled with 3 M KCl. All electrodes used measured 0.5–1.1 MΩ of resistance. The 10 mM Ba^{2+} (or Ca^{2+}) recording solution contained: 10 mM $Ba(OH)_2$ (or $Ca(OH)_2$), 90 mM NaOH, 1 mM KOH, 5 mM HEPES (pH 7.4, adjusted with methanesulfonic acid). To remove any contamination from Ca^{2+}-activated chloride currents, we injected the oocytes with 50 nL of 50 mM BAPTA (1,2-bis[o-aminophenoxy]

ethane -N,N,N',N'-tetraacetic acid) 30–60 min prior to recording. This was especially important while recording Ca^{2+} currents. Currents were sampled at 5 kHz and low pass filtered at 1 kHz using the pClamp system (Digidata 1320A and pClamp 8; Axon instruments, Foster City, CA, USA) unless otherwise noted.

We used whole cell patch clamp recordings from HEK-293 cells transiently transfected with Ca-α1T to measure tail currents. These recordings were obtained at room temperature using an Axopatch 200A amplifier connected to a computer through a Digidata 1300 A/D converter and controlled with the pCLAMP 9.2 software. Tail currents were recorded in a 10 mM Ba^{2+} solution containing the following: 140 mM TEACl, 2.5 mM CsCl, 10 mM $BaCl_2$, 1 mM $MgCl_2$, 10 mM glucose, and 10 mM HEPES (pH 7.3, adjusted with TEAOH). The pipette solution contained the following: 130 mM CsCl, 10 mM EGTA, 5 mM MgATP, 1 mM NaGTP, and 10 mM HEPES (pH 7.4, adjusted with CsOH). Recording pipettes were prepared from TW-150-3 capillaries (World Precision Instruments, Inc., Sarasota, FL). The pipette resistance was 2.0 ~ 3.0 MΩ. Access resistance was compensated by 70–80% using the compensation circuit and series resistance prediction. Tail current data were filtered at 10 kHz and digitized at 20 kHz. Peak currents and exponential fits were analyzed using the Clampfit software package (Axon instruments, Foster City, CA, USA). The activation and inactivation time constants for the T-type currents elicited by step pulse protocols were estimated by fitting individual current traces with double exponential functions: $A_1(1 - exp(-t/\tau_1)) + A_2(1 - exp(-t/\tau_2))$ where A_1 and A_2 are the coefficients for the activation and inactivation exponentials, t is time, and τ_1 and τ_2 are the activation and inactivation time constants, respectively. The smooth curves for channel activation and steady-state inactivation were obtained by fitting the data with a Boltzmann equation: $1/\{1 + exp[(V_{50} - V)/S_{act}]\}$, where V_{50} is the potential for half-maximal activation and S_{act} is the slope conductance. Dose-response curves for Ni^{2+} inhibition of T-type channel currents were derived by fitting the data using a Hill equation: $B = 1/(1 + IC_{50}/[Ni^{2+}]^n)$, where B is the normalized block, IC_{50} is the concentration of Ni^{2+} giving half maximal blockade, and n is the Hill coefficient.

Generation of knock-in alleles. 5′ and 3′ homologous arms surrounding the *Ca-α1T* locus were PCR-amplified using w^{1118} genomic DNA with the following primers: 5′-CGAGATGAATTCTAGCCTCATCAACTGAGC-3′, 5′-CGAGATGCGGCCGCGAGCAAGCACTAATAGCA-3′, 5′-GAGATACTAGTCATGCTACAATGTCAGCA-3′, 5′-CGAGATCTCGAGGGCCACGTATAGGGATGC-3′. The homologous arms were then inserted into the *pGX-attP* vector (DGRC #1293). P{Donor} flies were generated by P-element based transgenesis of *pGX-attP* containing the homologous arms into the w^{1118} genetic background (Genetic Services, Inc., US) and crossed to Flp I-Sce I flies for homologous recombination. Candidates for proper targeting (i.e., flies with red or mosaic eyes) were selected and verified by PCR. The *white* marker was removed from a verified strain via Cre-mediated recombination. The resulting $white^-$ line was used as a founder ($Ca\text{-}\alpha1T^{Founder,\ w-}$) for site-specific DNA integration. $Ca\text{-}\alpha1T^{Gal4}$, $Ca\text{-}\alpha1T^{Rescue}$ and *GFP::Ca-α1T* lines were generated by ϕC31 integrase-mediated site-specific integration. The Gal4 insert (i.e., splice acceptor-Gal4 CDS-poly A) was amplified from the *pBS-KS-attB1-2-GT-SA-GAL4-Hsp70pA* vector (DGRC #1325) with the following primers: 5′-CGTACTCCACGAATTTCTAGAAGTCGATCCAACAT-3′ and 5′-ACCGGCGCGCCTCGACTCTAGAACTAGTGGATCTA-3′. The resulting amplified DNA fragment was sequenced and inserted into the $pGE\text{-}attB^{GMR}$ vector (DGRC #1295) using the EZ-FusionTM cloning kit (Enzynomics, South Korea). The Rescue insert was PCR amplified from w^{1118} genomic DNA with the following primers: 5′-GCAGAATTCAATCGATTCCATAGATCCGC-3′ and 5′-GCACTCGAGAATTTTGCAACAGGCAGCTA-3′. The resulting fragment was inserted into the EcoR I/Xho I site of the $pGE\text{-}attB^{GMR}$ vector. The GFP insert along with a (Gly-Gly-Ser)x4 linker was amplified from the *pBS-KS-attB1-2-PT-SA-SD-1-EGFP-FIAsH-StrepII-TEV-3xFlag* vector (DGRC #1306) with the following primers: 5′-GCACCCCAGAAAATGGTGTCCAAGGGCGAGGAGCT-3′ and 5′-CGCTGGCTGTGGCAGGGAACCTCCGCTTCCACCGC-3′. The resulting fragment was inserted downstream of the ATG start site in the Rescue construct by inverse PCR (5′-CTGCCACAGCCAGCGGCAGCG-3′, 5′-CATTTTCTGGGGTGCCAACTA-3′) using the 5X In-Fusion HD Enzyme Premix (Clontech). $pGE\text{-}attB^{GMR}$ vectors containing the Gal4, Rescue, and GFP-tagging constructs were injected into $Ca\text{-}\alpha1T^{Founder,\ w-}$ embryos (Rainbow Transgenic Flies, Inc., US) for ϕC31-mediated site-specific integration into the *attP* landing site in the Ca-α1T locus. The $Ca\text{-}\alpha1T^{Gal4}$ and $Ca\text{-}\alpha1T^{Rescue}$ lines were backcrossed to w^{1118} for more than 8 generations and their white-markers were removed before behavioral analysis.

Generation of deletion mutants of Ca-α1T using imprecise P-element excision. EP line G1047 from the Genexel collection was crossed to the transposase line (*Dr[1]/TMS,Sb,P[Δ2–3]*). Mosaic-eyed progeny were collected and crossed to an X chromosome balancer (*phl12/FM6*) to obtain candidate excision lines. These candidates were then verified by PCR and backcrossed to w^{1118} for more than 8 generations before continuing to the sleep analyses.

Antibody generation and western blotting. A polyclonal antisera against Ca-α1T was generated using antigen derived from the 302 C-terminal amino acids of Ca-α1T (cloning primers: 5′-GAATTCCAAATTAATCCAATCCGTA-3′, 5′-GCGGCCGCTTAGTCCATGGAGGATT-3′). His-tagged antigen was expressed in *E. coli*, purified and injected into rabbits to generate an immune response (YoungIn Frontier, South Korea). Western blot analyses were performed according to standard protocols using rabbit antisera obtained after the third Ca-α1T antigen boost. β-Actin-specific antibodies (Santa Cruz Biotechnology, sc-47778) were used for the loading control.

Immunohistochemistry. Adult female fly brains were dissected in PBS and fixed with 4% PFA for 30 minutes at room temperature. Fixed brain samples were washed with PAT3 solution (0.5% TritonX-100, 0.5% BSA in PBS) for 15 min 3 times and incubated in 5% normal goat serum for 2–3 hours at room temperature. After blocking, samples were incubated with primary antibodies diluted in 5% normal goat serum overnight at 4 °C. The samples

were then washed with PAT3 for 1 hour 2 times at room temperature and incubated with secondary antibodies diluted in 5% normal goat serum overnight at 4 °C. After washing off the secondary antibodies with PAT3 for 1 hour 2 times, the brain samples were mounted in Vectashield (H-1000, Vector Laboratories, Inc.) and visualized on a LSM-780 confocal microscope (Zeiss, Germany). Primary antibodies: rabbit anti-GFP (1:500, A11122, Invitrogen); anti-bruchpilot monoclonal (1:50, nc82, DSHB). Secondary antibodies: goat anti-rabbit Alexa 488 (1:300, A11008, Invitrogen); goat anti-mouse Alexa 568 (1:300, A11031, Invitrogen).

Sleep and locomotor behavior analysis. Fly sleep and locomotor behavior was measured with the *Drosophila* Activity Monitoring system (Trikinetics). For sleep analysis, 3–4 day-old female flies were placed individually into 65 mm X 5 mm glass tubes with one end filled with 2% agar/5% sucrose food and the other end plugged with cotton. We defined periods of activity as periods with a beam break frequency higher than 1 per minute and periods of sleep as periods during which no beam break occurred for at least 5 consecutive minutes[42]. After one day of habituation in an incubator (25 °C, 60% humidity), we used the "Counting Macro" software[43] to measure sleep over the course of 4 days—2 days of 12 hr:12 hr light-dark conditions and 2 days of continuous darkness. For experiments using the GeneSwitch technique, flies were maintained on normal food containing 500 μM RU486 (M8046, Sigma-Aldrich) dissolved in ethanol (1%) for two days prior to the experiment. Control flies were maintained on normal food containing only ethanol (1%). For the GeneSwitch experiments, flies were placed in 2% agar/5% sucrose food with or without 500 μM RU486. For sleep deprivation, activity monitors with 3–5 day-old female flies were placed in a Sleep Nullifying Apparatus (SNAP)[44] designed to rotate and give a swift mechanical stimulus twice per minute. After three days under 12 hr:12 hr light-dark conditions, flies were sleep-deprived for 24 hr and allowed to recover 12 hr. The percentage of lost sleep recovered (% Δ Sleep) was calculated by subtracting the baseline sleep (i.e., sleep during the light phase immediately before the deprivation day) from the amount of sleep during the recovery period and then dividing by sleep lost. We confirmed that each genotype lost 90% of their baseline sleep during the deprivation period and we included only flies with $\geq$70% sleep lost in the following calculations. For the circadian locomotor analyses, we measured the activity of 1–3 day-old male flies in 30 minute bins and analyzed the data using ClockLab (Actimetrics) and the Counting Macro[45]. Significance level for the χ^2 periodogram was set to $\alpha = 0.05$. Flies with a power of significance (P-S) $\geq$10 were considered rhythmic.

Quantitative real-time PCR. Male adult flies were maintained for 2 days under 12 h:12 h light-dark conditions and 2 days of continuous darkness. 120–150 fly heads were collected for each time point (CT0-CT20) during the second day of continuous darkness. Total RNA was extracted using Trizol (Invitrogen) and reverse transcribed using the RevertAid First Strand cDNA Synthesis Kit (Thermo Scientific). Quantitative real-time PCR was performed using the TOPreal qPCR 2× premix (RT500M, Enzynomics, South Korea). Expression levels of *period* were normalized to the level of *rp49*. Primers: *per* (5′-GACCGAATCCCTGCTCAATA-3′, 5′-GTGTCATTGGCGGACTTCTT-3′); *rp49* (5′-ATGACCATCCGCCCAGCATA-3′, 5′-GAGAACGCAGGCGACCGTTG-3′).

Statistical analysis. All statistical analysis was performed using R (version 3.2.0)[46] except for the analysis of the electrophysiological recordings, which was performed in GraphPad (San Diego, CA, USA). For comparisons between two genotypes, we used the Student's t-test or Welch's t-test as described in the figure legends. The Mann-Whitney U test was substituted when the data did not follow a normal distribution. For comparisons among three or more genotypes, we used the one-way ANOVA followed by the Tukey HSD post hoc test. When the data had unequal variance, we used Welch's one-way ANOVA followed by the Games-Howell post hoc test. We used the "car"[47] and "userfriendlyscience"[48] R packages to perform Levene's test for homogeneity of variance and the Games-Howell post hoc test, respectively.

References

1. Lee, J., Kim, D. & Shin, H.-S. Lack of delta waves and sleep disturbances during non-rapid eye movement sleep in mice lacking alpha1G-subunit of T-type calcium channels. *Proc. Natl. Acad. Sci. USA* **101,** 18195–18199 (2004).
2. Steriade, M., Dossi, R. C. & Nuñez, A. Network modulation of a slow intrinsic oscillation of cat thalamocortical neurons implicated in sleep delta waves: cortically induced synchronization and brainstem cholinergic suppression. *J. Neurosci.* **11,** 3200–3217 (1991).
3. Dossi, R. C., Nuñez, A. & Steriade, M. Electrophysiology of a slow (0.5-4 hz) intrinsic oscillation of cat thalamocortical neurones *in vivo*. *J. Physiol.* **447,** 215–234 (1992).
4. Talley, E. M. *et al.* Differential distribution of three members of a gene family encoding low voltage-activated (T-type) calcium channels. *J. Neurosci.* **19,** 1895–1911 (1999).
5. Ryglewski, S., Lance, K., Levine, R. B. & Duch, C. Ca(v)2 channels mediate low and high voltage-activated calcium currents in Drosophila motoneurons. *J. Physiol.* **590,** 809–825 (2012).
6. Perez-Reyes, E. *et al.* Molecular characterization of a neuronal low-voltage-activated T-type calcium channel. *Nature* **391,** 896–900 (1998).
7. Carbone, E. & Lux, H. A low voltage-activated, fully inactivating Ca channel in vertebrate sensory neurones. *Nature* **310,** 501–502 (1984).
8. Cribbs, L. L. *et al.* Cloning and characterization of alpha1H from human heart, a member of the T-type Ca^{2+} channel gene family. *Circ. Res.* **83,** 103–109 (1998).
9. Lee, J.-H. *et al.* Cloning and expression of a novel member of the low voltage-activated T-type calcium channel family. *J. Neurosci.* **19,** 1912–1921 (1999).
10. Klöckner, U. *et al.* Comparison of the Ca^{2+} currents induced by expression of three cloned α1 subunits, α1G, α1H and α1I, of low-voltage-activated T-type Ca^{2+} channels. *Eur. J. Neurosci.* **11,** 4171–4178 (1999).
11. Matteson, D. & Armstrong, C. Properties of two types of calcium channels in clonal pituitary cells. *J. Gen. Physiol.* **87,** 161–82 (1986).
12. McRory, J. E. *et al.* Molecular and functional characterization of a family of rat brain T-type calcium channels. *J. Biol. Chem.* **276,** 3999–4011 (2001).
13. Shcheglovitov, A., Kostyuk, P. & Shuba, Y. Selectivity signatures of three isoforms of recombinant T-type Ca^{2+} channels. *Biochim. Biophys. Acta, Biomembr.* **1768,** 1406–1419 (2007).
14. Lee, J.-H., Gomora, J. C., Cribbs, L. L. & Perez-Reyes, E. Nickel block of three cloned T-type calcium channels: low concentrations selectively block α1H. *Biophys. J.* **77,** 3034–3042 (1999).

15. Huang, J., Zhou, W., Dong, W., Watson, A. M. & Hong, Y. Directed, efficient, and versatile modifications of the Drosophila genome by genomic engineering. *Proc. Natl. Acad. Sci. USA* **106,** 8284–8289 (2009).
16. Astori, S. *et al.* The CaV3.3 calcium channel is the major sleep spindle pacemaker in thalamus. *Proc. Natl. Acad. Sci. USA* **108,** 13823–13828 (2011).
17. Hendricks, J. *et al.* Gender dimorphism in the role of cycle (BMAL1) in rest, rest regulation, and longevity in Drosophila melanogaster. *J. Biol. Rhythms.* **18,** 12–25 (2003).
18. Parisky, K. *et al.* PDF cells are a GABA-responsive wake-promoting component of the Drosophila sleep circuit. *Neuron* **60,** 672–82 (2008).
19. Osterwalder, T., Yoon, K. S., White, B. H. & Keshishian, H. A conditional tissue-specific transgene expression system using inducible GAL4. *Proc. Natl. Acad. Sci. USA* **98,** 12596–12601 (2001).
20. Senatore, A. & Spafford, J. D. Transient and big are key features of an invertebrate T-type channel (LCa_v3) from the central nervous system of Lymnaea stagnalis. *J. Biol. Chem.* **285,** 7447–7458 (2010).
21. Iniguez, J., Schutte, S. S. & O'Dowd, D. K. Cav3-type α1T calcium channels mediate transient calcium currents that regulate repetitive firing in Drosophila antennal lobe PNs. *J. Neurophysiol.* **110,** 1490–1496 (2013).
22. Kang, H. *et al.* A molecular determinant of nickel inhibition in Cav3.2 T-type calcium channels. *J. Biol. Chem.* **281,** 4823–30 (2006).
23. Park, H. *et al.* Asp residues of the Glu-Glu-Asp-Asp pore filter contribute to ion permeation and selectivity of the Ca(v)3.2 T-type channel. *Cell Calcium* **54,** 226–35 (2013).
24. Anderson, M. P. *et al.* Thalamic Cav3.1 t-type Ca^{2+} channel plays a crucial role in stabilizing sleep. *Proc. Natl. Acad. Sci. USA* **102,** 1743–1748 (2005).
25. Kraus, R. L. *et al. In vitro* characterization of T-type calcium channel antagonist TTA-A2 and *in vivo* effects on arousal in mice. *J. Pharmacol. Exp. Ther.* **335,** 409–417 (2010).
26. Senatore, A., Zhorov, B. S. & Spafford, J. D. Cav3 T-type calcium channels. *WIREs Membr. Transp. Signal.* **1,** 467–491 (2012).
27. Shang, Y. *et al.* Imaging analysis of clock neurons reveals light buffers the wake-promoting effect of dopamine. *Nat. Neurosci.* **14,** 889–895 (2011).
28. Young, J. M. & Armstrong, J. D. Structure of the adult central complex in Drosophila: organization of distinct neuronal subsets. *J. Comp. Neurol.* **518,** 1500–1524 (2010).
29. Lin, D. M. & Goodman, C. S. Ectopic and increased expression of Fasciclin II alters motoneuron growth cone guidance. *Neuron* **13,** 507–523 (1994).
30. Kitamoto, T. Conditional modification of behavior in Drosophila by targeted expression of a temperature-sensitive shibire allele in defined neurons. *J. Neurobiol.* **47,** 81–92 (2001).
31. Sakai, T. & Kitamoto, T. Differential roles of two major brain structures, mushroom bodies and central complex, for Drosophila male courtship behavior. *J. Neurobiol.* **66,** 821–834 (2006).
32. Connolly, J. B. *et al.* Associative learning disrupted by impaired Gs signaling in *Drosophila* mushroom bodies. *Science* **274,** 2104–2107 (1996).
33. Zars, T., Fischer, M., Schulz, R. & Heisenberg, M. Localization of a short-term memory in *Drosophila*. *Science* **288,** 672–675 (2000).
34. Renn, S. C., Park, J. H., Rosbash, M., Hall, J. C. & Taghert, P. H. A pdf neuropeptide gene mutation and ablation of PDF neurons each cause severe abnormalities of behavioral circadian rhythms in *Drosophila*. *Cell* **99,** 791–802 (1999).
35. Friggi-Grelin, F. *et al.* Targeted gene expression in *Drosophila* dopaminergic cells using regulatory sequences from tyrosine hydroxylase. *J. Neurobiol.* **54,** 618–627 (2003).
36. Freeman, M. Reiterative use of the EGF receptor triggers differentiation of all cell types in the Drosophila eye. *Cell* **87,** 651–660 (1996).
37. Glossop, N. R. *et al.* VRILLE feeds back to control circadian transcription of Clock in the *Drosophila* circadian oscillator. *Neuron* **37,** 249–261 (2003).
38. Rulifson, E. J., Kim, S. K. & Nusse, R. Ablation of insulin-producing neurons in flies: growth and diabetic phenotypes. *Science* **296,** 1118–1120 (2002).
39. Alekseyenko, O. V., Lee, C. & Kravitz, E. A. Targeted manipulation of serotonergic neurotransmission affects the escalation of aggression in adult male *Drosophila melanogaster*. *PLoS One* **5,** e10806 (2010).
40. Renn, S. C. *et al.* Genetic analysis of the *Drosophila* ellipsoid body neuropil: organization and development of the central complex. *J. Neurobiol.* **41,** 189–207 (1999).
41. Taghert, P. H. *et al.* Multiple amidated neuropeptides are required for normal circadian locomotor rhythms in Drosophila. *J. Neurosci.* **21,** 6673–6686 (2001).
42. Shaw, P. J., Cirelli, C., Greenspan, R. J. & Tononi, G. Correlates of sleep and waking in Drosophila melanogaster. *Science* **287,** 1834–1837 (2000).
43. Pfeiffenberger, C., Lear, B., Keegan, K. & Allada, R. Processing sleep data created with the Drosophila Activity Monitoring (DAM) System. *Cold Spring Harb. Protoc.* **2010,** pdb.prot5520 (2010).
44. Shaw, P. J., Tononi, G., Greenspan, R. J. & Robinson, D. F. Stress response genes protect against lethal effects of sleep deprivation in drosophila. *Nature* **417,** 287–291 (2002).
45. Pfeiffenberger, C., Lear, B., Keegan, K. & Allada, R. Processing circadian data collected from the Drosophila Activity Monitoring (DAM) System. *Cold Spring Harb. Protoc.* **2010,** pdb.prot5519 (2010).
46. R Core Team. *R: A Language and Environment for Statistical Computing*. R Foundation for Statistical Computing, Vienna, Austria (2015).
47. Fox, J. & Weisberg, S. *An R Companion to Applied Regression* (Sage, Thousand Oaks CA, 2011), second edn.
48. Peters, G.-J. *userfriendlyscience: Quantitative analysis made accessible* (2015). R package version 0.3-0.
49. Park, J.-Y. *et al.* Activation of protein kinase C augments T-type Ca^{2+} channel activity without changing channel surface density. *J. Physiol.* **577,** 513–523 (2006).
50. Park, J., Kang, H., Jeong, S. & Lee, J. Multiple structural elements contribute to the slow kinetics of the Cav3.3 T-type channel. *J. Biol. Chem.* **279,** 21707–13 (2004).
51. Demers-Giroux, P., Bourdin, B., Sauvé, R. & Parent, L. Cooperative activation of the T-type $Ca_v3.2$ channel: interaction between Domains II and III. *J. Biol. Chem.* **288,** 29281–93 (2013).
52. Chemin, J. *et al.* Specific contribution of human T-type calcium channel isotypes (alpha(1G), alpha(1H) and alpha(1I)) to neuronal excitability. *J. Physiol.* **540,** 3–14 (2002).

Acknowledgements

K.J. would like to thank Sujin Chae for helpful technical assistance. This work was supported by the Priority Research Centers Program of the National Research Foundation of the Republic of Korea (2012-0006690) to J.-H.L., by the Intelligent Synthetic Biology Center of Global Frontier Project funded by the Ministry of Science, ICT and Future Planning (2011-0031955) to D.K., and by grants from the National Research Foundation of the Republic of Korea to D.K. (NRF-2011-0028772), J.C. (NRF-2015-021435) and W.D.J. (2013R1A1A2011339).

Author Contributions

K.J., J.C., J.-H.L., D.K. and W.D.J. designed research. K.J., H.S. and S.L. performed the research. K.J., H.S., S.L., Y.O., D.J. and W.D.J. analyzed the data. K.J., J.-H.L., D.K. and W.D.J. wrote the paper.

Additional Information

Supplementary information accompanies this paper at http://www.nature.com/srep

Competing financial interests: The authors declare no competing financial interests.

How to cite this article: Jeong, K. *et al.* Ca-α1T, a fly T-type Ca^{2+} channel, negatively modulates sleep. *Sci. Rep.* **5**, 17893; doi: 10.1038/srep17893 (2015).